Acta Materialia 135 (2017) 103–111

Contents lists available at ScienceDirect

Acta Materialia

journal homepage: www.elsevier.com/locate/actamat

Full length article

Nonstoichiometric [012] dislocation in strontium titanate

Yuho Furushima [a], Yuki Arakawa [a], Atsutomo Nakamura [a, *], Eita Tochigi [b], Katsuyuki Matsunaga [a, c]

[a] Department of Materials Science and Engineering, Nagoya University, Furo-cho, Chikusa-ku, Nagoya 464-8603, Japan
[b] Institute of Engineering Innovation, The University of Tokyo, 2-11-16, Yayoi, Bunkyo-ku, Tokyo 113-8656, Japan
[c] Nanostructures Research Laboratory, Japan Fine Ceramics Center, 2-4-1, Mutsuno, Atsuta-ku, Nagoya 456-8587, Japan

ARTICLE INFO

Article history:
Received 8 October 2016
Received in revised form
13 May 2017
Accepted 8 June 2017
Available online 9 June 2017

Keywords:
Dislocations
Stacking fault
Electron microscopy
DFT calculations
$SrTiO_3$

ABSTRACT

Dislocations are one-dimensional lattice defects in crystalline materials, and unique atomic configurations at their core can affect functional properties of materials. Here we report on a [012] dislocation having a nonstoichiometric core structure in strontium titanate ($SrTiO_3$). TEM and STEM observations showed that a (001) low-angle tilt grain boundary consists of two types of dislocations. One is a [001] edge dislocation that compensates a tilt angle of the boundary as found in previous studies. The other is a [012] dislocation with both edge and screw component. This dislocation is considered to be formed to compensate a slight twist angle of the boundary. It is interesting that the [012] dislocations have a specific core structure with the dissociation into three partial dislocations of $\boldsymbol{b} = 1/2$ [011], [001] and 1/2 [011]. At stacking faults formed with the dissociation, two (001) Ti-O layers were located to be neighbors across the stacking fault plane due to missing of a (001) Sr-O layer. In addition, the energy of the stacking fault was estimated to be 0.4 J/m^2 from the separation distances between partial dislocations. It is suggested that the [012] dislocation is formed due to presence of the nonstoichiometric stacking fault structure with low energy.

1. Introduction

Dislocations in oxide crystals have attracted much attention because of their effects on the bulk properties, including ionic [1–3] and electronic [4–14] transportation properties. An atomic configuration at a dislocation core differs remarkably from that in the bulk, and a strain field is also present around a dislocation. Such characteristics of dislocation have a potential to induce unique physical properties. To date, a great number of studies have been done by using bicrystals with low-angle grain boundaries to investigate the structures and properties of dislocations [7–26]. In general, low-angle tilt grain boundaries consist of edge dislocations with a Burgers vector perpendicular to the boundary plane, while low-angle twist grain boundaries consist of screw dislocations with a Burgers vector in the boundary plane. Accordingly, experimental studies using bicrystals are useful to investigate structures and properties of dislocations because dislocation characters introduced at the boundary can be artificially controlled.

Strontium titanate ($SrTiO_3$) has the cubic perovskite structure with space group *Pm*3*m*, and is widely used as functional materials for ceramic capacitors, varistors and so on. It is considered that these applications rely on the presence of space-charge layers in the vicinity of the grain boundaries [7–12,27–29]. Since boundary dislocations in $SrTiO_3$ are also believed to play an essential role in such electrical properties, they have been the focus of many studies using bicrystals [7–12,15–22]. Particularly, the structures of [001] edge dislocations at the (001)/[010] low-angle tilt grain boundaries have been keenly studied using conventional transmission electron microscopy (TEM), high resolution TEM (HRTEM), and scanning TEM (STEM) [19–22]. These observations revealed a variety of core structures in the [001] dislocations. Additionally, it has been reported that the (001)/[010] low-angle tilt grain boundaries, which consist of the [001] dislocations, can affect the electrical resistance behavior of the crystal [7–12].

In this study, $SrTiO_3$ bicrystals with a (001)/[010] 4° tilt grain boundary were fabricated, and dislocation structures at the boundary were observed by TEM and STEM. It was found that dissociated dislocations with a large Burgers vector of $\boldsymbol{b} =$ [012] are periodically formed at the boundary in addition to the [001]

* Corresponding author. Building 5. of Graduate School of Engineering, Furo-cho, Chikusa-ku, Nagoya 464-8603, Japan.
E-mail address: anaka@nagoya-u.jp (A. Nakamura).

http://dx.doi.org/10.1016/j.actamat.2017.06.017
1359-6454/

dislocations. This paper addresses the atomic structure of the [012] dislocations in detail on the basis of the observation results and theoretical calculations.

2. Experimental procedure and computational method

$SrTiO_3$ bicrystals with 4° (001)/[010] symmetrical tilt grain boundaries were fabricated by diffusion bonding. For the bicrystal fabrication, two single crystal plates inclined at +2° and −2° from the (001) plane around the [010] axis were prepared. The size of the single crystal plates was 10 × 10 × 1 mm^3, and the surfaces of the plates were polished by diamond slurry to achieve a mirror finish. The two single-crystal plates were joined by diffusion bonding at 1000 °C in air for 10 h under a uniaxial load of 10 N. After that, the fabricated bicrystals were annealed at 1500 °C in air for 10 h in order to attain sufficient atomic diffusion. Specimens for TEM observation were prepared by standard techniques including Ar^+ ion milling. The grain boundary dislocations were observed using a conventional TEM (HITACHI H-800, 200 kV) and STEM (JEOL JEM-ARM200F, 200 kV).

Energies of (001) stacking faults associated with dissociation of the dislocations were evaluated by using density-functional theory (DFT) calculations in order to determine the stable stacking fault structure. All calculations were performed by the projector augmented wave (PAW) method as implemented in the Vienna Ab-initio Simulation Package (VASP) code [30]. The generalized gradient approximation (GGA) was selected for the exchange correlation potential [31]. Sr 4*s*4*p*5*s*, Ti 3*p*4*s*3*d* and O 2*s*2*p* electrons were described as valence electrons. To make a correction of on-site Coulomb interactions of 3*d* orbitals of Ti atoms, the GGA + *U* method [32] was applied with parameters of $U = 5.0$ eV and $J = 0.64$ eV [33]. Wave functions were expanded by plane waves with a cut-off energy of 600 eV. For calculation of stacking fault energies, the supercells including 36 atoms and two equivalent stacking faults were used with periodic boundary conditions. In this case, the separation distance between repeated stacking faults corresponds to 1.4 nm. Brillouin zone integration was carried out using a 6 × 6 × 1 *k*-point grid. Structure optimization was conducted until residual atomic forces reached to less than 0.01 eV/Å. Details of the supercell structure will be also described in the following section.

3. Results and discussion

Fig. 1(a) shows a typical dark field TEM image of the (001)/[010] 4° tilt grain boundary taken using $\boldsymbol{g} = 002$. The boundary mainly consisted of the dot like contrasts (shown in the red box in Fig. 1(a)). They were arranged with an interval of 5.6 nm along the boundary. Meanwhile, the expanded contrasts shown in the blue box on Fig. 1(a) were also periodically formed along the [100] direction at the boundary. The blue arrows in Fig. 1(a) indicate the positions of the expanded contrasts. It can be seen from the image that they appear with large faint contrasts at an equal interval of 73 nm. Fig. 1(b) and (d) represent selected-area diffraction (SAD) patterns from on the grain boundary, the upper grain and the lower grain, respectively, which were taken approximately along the [010] zone axis. Here note that these SAD patterns were acquired by changing the position of the SA aperture on the same field of view without moving the specimen in the TEM. As can be seen from Fig. 1(b), the spots originating from both the two grains were separated from each other. From the separation, the tilt angle of the boundary was estimated to be approximately 4°, which coincides with the designed tilt angle. Moreover, the intensities of the diffraction spots on the SAD patterns in Fig. 1(c) and (d) do not display perfect four-fold symmetry: in Fig. 1(c) the diffraction spots

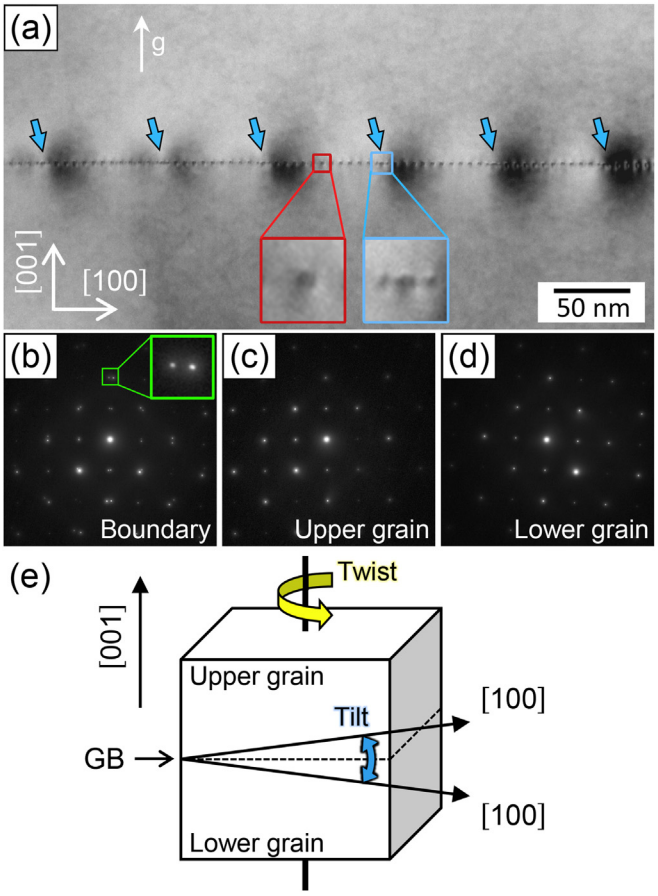

Fig. 1. (a) A dark-field TEM image of the grain boundary taken using $g = 002$. (b) A selected-area diffraction (SAD) pattern obtained from on the boundary. The part enclosed by the green box is an enlargement of the diffraction spots. (c), (d) SAD patterns obtained from the upper and lower grains, respectively. (e) Schematic illustration of crystallographic orientation relationship of the fabricated grain boundary. The blue and yellow arrows represent tilt and twist misorientations of the boundary. (For interpretation of the references to colour in this figure legend, the reader is referred to the web version of this article.)

in the left half part are brighter than ones in the right half part, whereas in Fig. 1(d) ones in the right half part are brighter. This implies that the orientations of these two grains are slightly rotated around the [001] axis each other, corresponding to a twist misorientation of the grain boundary. This can be due to a slight misalignment in the fabrication process of a bicrystal. Crystallographic orientation relationship of the fabricated grain boundary is schematically shown in Fig. 1(e).

In order to investigate the twist misorientation of the boundary in more detail, crystal orientation analysis was performed using the central zero-order disc of the convergent beam electron diffraction pattern in the forward scattered beam, which is known as Ronchigram. A Ronchigram contains information on crystallographic orientation relationship [34]. Fig. 2(a) shows a high-angle annular dark-field STEM (HAADF-STEM) image used for this analysis. Fig. 2(b) shows the Ronchigrams derived from the points labeled by A, B, C and D in Fig. 2(a). The points A and B are located on the upper grain (5 nm above the boundary), while the points C and D are located on the lower grain (5 nm below the boundary). Here, the red, green, blue and orange dashed lines drawn on the obtained Ronchigrams correspond to the Kikuchi patterns [35]. Accordingly, the intersections of the lines represent the [010] zone axes. The illustrations on the right hand side of Fig. 2(b) show the overlapped